17th Brazilian Congress of Thermal Sciences and Engineering
November 25th-28th, 2018, Águas de Lindóia, SP, Brazil

ENCIT-2018-0334
STATIC TORQUE MEASUREMENT ON A MULTI DISK TURBINE

André Luis Ribeiro Thomazoni
Federal University of Rio Grande do Sul, Porto Alegre, Brazil
andrethomazoni@gmail.com

Ruddy Bazan Antequera
Federal University of Rio Grande do Sul, Porto Alegre, Brazil
ing.baz.ant@gmail.com

Paulo Smith Schneider
Federal University of Rio Grande do Sul, Porto Alegre, Brazil
pss@mecanica.ufrgs.br

Abstract. *Multi disk turbine MDT is a bladeless device that allows to convert energy from low energy availability streams. In this study, the static torque of an laboratory MDT prototype is measured for different rotor configurations under 5 inlet air pressure levels. Rotor is assembled with 5 different disk number, from 0 to 4 parallel disks (Type A assembling) followed by a study of spacing combination with 2 disks (Type B assembling). 35 tests in choked flow condition are presented and the influence of the number of disks represents a 50% enhancement of the initial static torque value. Disks spacing also displays a static torque increment of 17%. Taking into account only the effect of increasing the inlet pressure, results show a rise in torque up to 2.45 times its initial value. Finally, considering all the effects together, torque increased from 0.28Nm to 1.2Nm, which is a rise of around 4 times its initial value.*

Keywords: *Tesla turbine, Multiple Disk Turbine, Stall torque*

Nomenclature

F	Force on load cell [N]
L	Lever arm for torque measurement [m]

Greek symbols

τ	Torque [Nm]

1. INTRODUCTION

Multi disk turbines MDT are bladeless devices patented by Nikola Tesla (1856–1943) in 1913, and became known as Tesla turbine. The turbine rotor is made of a series of co-rotating parallel flat disks, closely spaced and attached to a central shaft (Sengupta and Guha, 2012). Tesla turbines can work as conversion devices when driven by several types of fluids, but also be motorized to pump or compress fluids streams. Its simple conception allows it to work with non-treated fluids, and displays a relative lower manufacturing cost compared to regular turbines. Those characteristics make then suitable for low-cost solution and energy recovery (Usman Saeed Khan *et al*, 2013, Hasan, 2016).

Several authors have been studying its design, application, and performance with numerical and experimental approaches (Cairns, 2003; Couto, 2006; Lemma et al., 2008 and Maidana, 2015). Rice (1965) performed experiments with several MDTs and pointed out the device suitability to MDT applications on low grade energy streams. Truman (1985) conducted a numerical investigation of turbulent flow between two disks to predict the velocity field as a function of the Reynolds number, under stationary or co-rotating schemes. Lemma *et al* (2008) developed a combined experimental and numerical study on the MDT performance, and found out that these devices may find use in applications such as small power sources for electronic appliances and micro-combined heat and power applications, with adiabatic experimental and numeric efficiencies around 25% and 40%, respectively. Emram (2011) proposed two analytic methods to assess torque behavior. Then the author compares the methods results with so called “preliminary experiments” in order to extrapolate the turbine performance over a set of parameters, which allowed him to design both a MDT and an electrodynamometer. As a conclusion, it was found that the analytic methods were sufficient to define the upper and lower bounds of theoretical static torque. Holland, (2015) designed and constructed a MDT prototype with 92mm of diameter, central exhaust, plenum chamber, and swappable nozzles. The author found a MDT maximum efficiency of 8.5% and torque values form stall condition ranging from 0.15Nm to 0.31Nm in their experiments.

According to the literature review, the behavior of MDT under complete break condition, or static rotor condition, has not yet been largely explored by previous researchers. Based on that lack of knowledge, the goal of the present work is to measure the static torque from a small scale MDT under complete break condition in order to better identify the influence of geometric changes in rotor configuration for a range of inlet pressure levels.

2. TURBINE DESCRIPTION

The same Multi Disk Turbine MDT working prototype presented by Ermel et al (2017) was used to perform the set of controlled essays reported in this paper, aiming to study the influence of the number of rotor disks and their placement on the MDT performance. Its housing was made of machined steel, nozzle in stainless steel and rotor disks in aluminum. Deep-grove ball bearings were selected to work with angular speed up to 22.000rpm and to be axially fixed to the housing, keeping the rotor gap aligned with the TMD nozzle.

MDT rotor was designed operate with variable number and placement of internal parallel disks. Its basic structure is presented in Fig 1(a), composed by two 3mm external disks, 300mm external diameter and 100mm internal diameter, leaving a 9mm internal gap. Internal 1mm thick disks can be placed in different number and positions, as shown in Fig 1(b).

(a) (b)

Figure 1. Rotor assembling with (a) External disks and (b) with 4 internal disks.

Table 1 presents the 7 rotor configurations that were tested in the present work, based on the same structure displayed in Fig. 1(a), labeled as 0.

Table 1. MDT 7 rotor disks assemblies

Internal disks	Image	Spacing	Label	Internal disks	Image	Spacing	Label
0 Disk		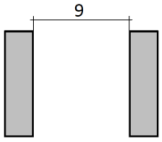	0	2c Disks	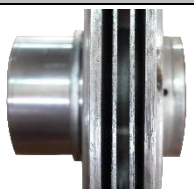	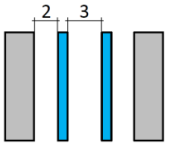	IoI
1 Disk		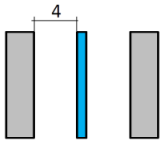	I	3 Disks		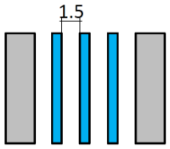	III
2a Disks		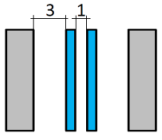	II	4 Disks		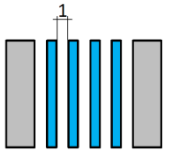	IIII
2b Disks		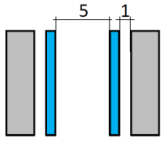	IOI				

Turbine was equipped with a single convergent shaped rectangular nozzle (Fig. 2), with a 75mm^2 inlet area (7.5mm length; 10mm height) and with a 30mm^2 outlet area (7.5mm length; 4mm height). Its outlet area was designed to be in accordance to the rotor 9mm gap, with adjustable attack angles, and aiming to avoid fluid leak along disks and housing.

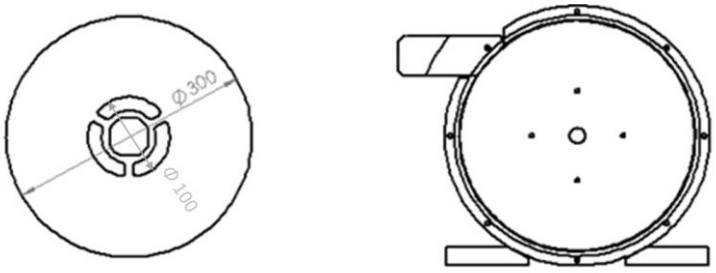

(a) (b)

Figure 2. (a) Disk front view and (b) nozzle placement on the MDT casing

3. WORKBENCH DESCRIPTION

The MDT was assembled in a workbench (Fig. 3) to be driven by compressed air at different pressure and temperature levels.

a) b)

Figure 3. Workbench (a) front and (b) rear views (Ermel et al, 2017)

Data acquisition was designed to capture and treat signals depicted in Fig. 4. Sensors and captors were connected to a Labview[1] application and fluid thermodynamic properties calculated with the aid of EES[2] tables. Fluid mass flow rate, torque and error propagation were also estimated by that last software.

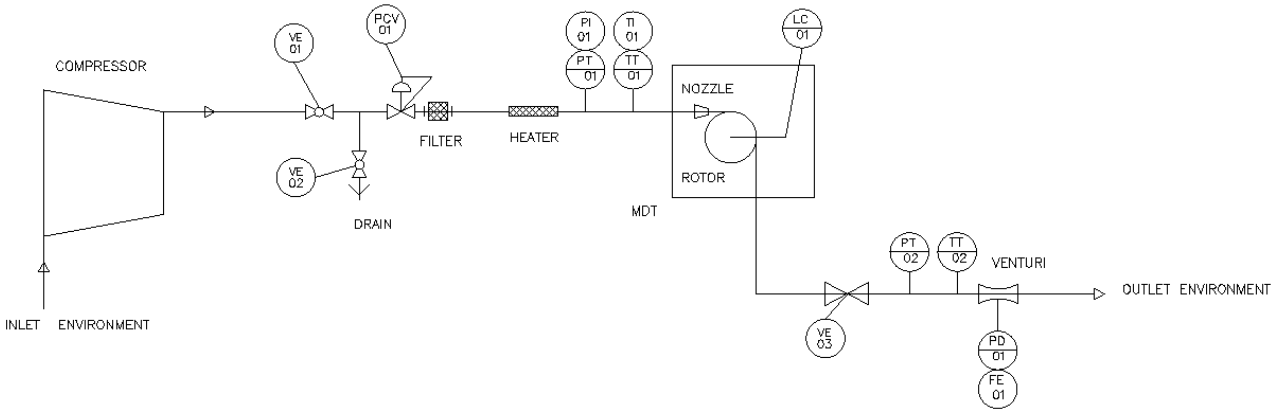

Figure 4. Workbench instrument layout

[1] www.ni.com
[2] www.fchart.com

Filtered air was adopted as the working fluid, fed by a dedicated compressor and conditioned by a control valve. Air inlet pressure was set by valve *PCV-01*, inlet temperature through the heater control[3] and the fluid pressure and temperature measured by *PT-01*, *PT-02*, *TT-01* and *TT-02*. The dashed line around the MDT area represents the turbine, composed by its nozzle, housing and rotor. Tags indicate instruments and sensors along the flow line, as manometers, thermometers, volumetric-flow meters, etc. Workbench main sensors and instruments are declared and described in Table 2, following the tag labels presented in Fig. 4.

Table 2. Workbench components, according to Fig 4

TAG	Description	Model	Range	Uncertainty
PI-01	Manometer (main line)	-	0 to 17bar	-
VE-01	Sphere valve ½" – Inlet 1	-	-	-
PCV-01	Pressure control valve	Norgren R17	0.3 to 8.5bar	
TI-01	Temperature display (analogic)	-	0 to 200°C	-
VE-02	Sphere valve ½" – Inlet 2	-	-	-
TT-01	Temp. transmitter – Nozzle inlet	Type K thermocouple	-200 to 1250°C	± 0.5°C
PT-01	Pressure transmitter – Nozzle inlet	PS-10B	0 to 10bar	± 8823Pa
LC-01	Load cell	Bonad - Bnd - Ic5.0	1N	± 0.0001N (0.001%FS)
VE-03	Gate valve 2"	-	-	-
FE-01	Primary flow element – Venturi	-	-	-
PD-01	Differential pressure sensor	MPXV7002	-2 to 2kPa	± 50.9Pa
PT-02	Pressure sensor – System outlet	MPX4115	15 to 115kPa	± 12571Pa
TT-02	Temp. sensor – System outlet	Type K thermocouple	-200 to 1250°C	± 0.61°C

FS = full scale

Pressure sensors *PT-01* and *PT-02* were placed along the pipe internal surface in order to capture fluid static pressure, and temperature sensors *TT-01* and *TT-02* at the center of pipe cross sectional area. Fluid flow rate was determined using a Venturi device builted accordlying with NBR 5167-1:2008, equipped with a differential pressure sensor *PD-01*, *TT-02* and *PT-02* values were used to determine the thermodynamic state at Venturi inlet.

Turbine torque was measured by a load cell assembled to an external disk mounted in MDT shaft (Fig. 5) .

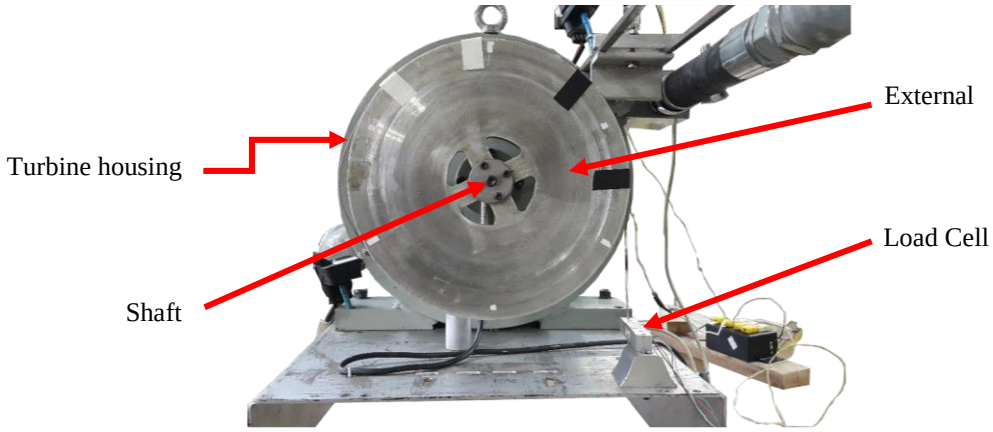

Figure 5. MDT torque measurement

The experimental value for torque τ was calculated by Eq. (1), as follows:

$$\tau = F\,L \tag{1}$$

with F the experimental force measured in the load cell LC-01 and L is the lever arm 0.125m long.

4. RESULTS

Tests were performed for all disk configurations presented in Table 1 by varying compressed air absolute inlet pressure from 200 to 400kPa (*PCV-01*) while the inlet temperature was kept constant at 296K with the aid of an air heater. All sensor outputs displayed in Fig. 4 were acquired at an 1 second rate under steady state conditions. More than 15,000 readings were collected and spurious values were withdrawn bu applying the Chauvenet criteria. Average values of the measured data are presented in Table A.1– Appendix A, for 35 test sequences.

[3] Novus CLP-n1200 https://www.novus.com.br/downloads/Arquivos/manual_n1200_v20x_d_portuguese.pdf

Before analyzing the tests results, some preliminary assessments were performed to identify the bench capability of reproducing inlet and outlet pressure leves, as follows:

- Inlet air pressure reproducibility, aiming to verify the deviation limits of each pressure level;
- Outlet air pressure state;
- Air mass flow rate, and chocked flow conditions.

Regarding geometrical disk configuration, tests results were organized in two types:

- Type A: variable number of disks, (rotors labeled 0, I, II, III and IIII) to assess the influence of area in momentum transfer;
- Type B: 2 disks placed according to labels II, I0I and IoI, to assess momentum transfer for constant area at different disk position;

Finally, it was assessed the static torque behavior as function of the inlet pressure.

4.1 INLET AIR PRESSURE REPRODUCIBILITY

Table 3 presents results obtained from controled test performed to verify the inlet air reproducibility condition. A sequence of tests were performed with each of the 7 rotor configurations, declared in Table 1, in order to verify the dispertion on the inlet air pressure produced by control valve *PCV-01*. Sensor uncertainties are *PT-01* = ± 8823Pa and *TT-01* = ± 0.5K, as declared in Table 2.

Table 3. Inlet air pressure and temperature for 5 inlet absolute pressure levels and fixed temperature

Run	**1**		**2**		**3**		**4**		**5**	
Sensor tag	**PT-01**	**TT-01**	**PT-01**	**TT-01**	**PT-01**	**TT-01**	**PT-01**	**TT-01**	**PT-01**	**TT-01**
Unit	**[Pa]**	**[K]**	**[Pa]**	**[K]**	**[Pa]**	**[K]**	**[Pa]**	**[K]**	**[Pa]**	**[K]**
Label 0	203089	296.8	252222	297.1	299759	296.7	349545	296.6	402056	296.9
Label I	202490	297.5	251693	296.7	302795	296.6	351323	296.4	398853	296.4
Label II	202798	297.5	252311	297.3	304053	297.0	352976	296.9	401981	296.8
Label I0I	201516	296.4	252850	295.9	300646	295.6	352584	295.7	399788	296.0
Label IoI	201605	296.6	251834	296.4	302329	296.3	351143	296.2	401480	296.3
Label III	202310	297.1	251521	296.8	300360	296.6	350161	296.8	402271	297.3
Label IIII	200377	296.8	252000	296.4	302862	296	351720	296.2	399400	297.0
Mean	202026	297.0	252062	297.0	301829	296.0	351350	296.0	400833	297.0
Standard deviation	±929	±0.3	±446	±0.5	±1583	±0.5	±1226	±0.4	±1436	±0.4
Span	2712	1.1	1329	1.4	4294	1.4	3431	1.2	3418	1.0

One can be observe that the inlet pressure standard deviation was quite lower than the corresponding pressure and temperature mean values. This is an indication that, for each run, the preset pressure values were reproduced by the control system – *PCV-01*.

Span values to the difference among the maximum and minimum measured value, and were compared to the corresponding measurement uncertainty. The higher pressure span value was found for Run 3, with 4294Pa, which corresponds to half of the sensor uncertainty. That observation, together with the value of the Standard deviation, allows concluding that pressure inlet uncertainty at *PT-01* should be improved. Even though, it is correct to state that the difference among , set to 50.000kPa, are big enough to be considered outside of the sensor uncertainty range (±8823Pa). Temperature span was always higher than the sensor uncertainty, more likely due to the fluctuation of the compressed air supply and to environmental conditions, and a more stable temperature control could be achieved by turning on the workbench heater to a few degrees above room conditions. On the present work, temperature sensor *TT-01* uncertainty was assumed to be ±0.7K to artificially express air temperature fluctuation.

4.2 OUTLET AIR PRESSURE STATE

Similarly to the former assessment of inlet compressed air levels, the outlet air state was measured for the same inlet pressure leves to calculate the optputs mean valuea, the Standard deviationa and the span, displayed in Table 4. Sensor uncertainties are *PT-02* = ± 12571Pa and *TT-02* = ± 0.6K, as declared in Table 2.

Table 4. Outlet air pressure and temperature for 5 inlet absolute pressure levels and fixed temperature

Run	**1 (200 kPa)**		**2 (250 kPa)**		**3 (300 kPa)**		**4 (350 kPa)**		**5 (400 kPa)**	
Sensor tag	**PT-02**	**TT-02**	**PT-02**	**TT-02**	**PT-02**	**TT-02**	**PT-02**	**TT-02**	**PT-02**	**TT-02**
Unit	**[Pa]**	**[K]**	**[Pa]**	**[K]**	**[Pa]**	**[K]**	**[Pa]**	**[K]**	**[Pa]**	**[K]**
Label 0	102467	296.66	102460	296.78	102513	296.37	102555	296.69	102629	297.55
Label I	102629	296.65	102669	296.39	102715	296.21	102757	296.04	102813	296.03
Label II	101938	297.17	101988	296.95	102052	296.69	102114	296.51	102172	296.41
Label I0I	102638	296.07	102679	295.56	102738	295.14	102791	295.48	102859	295.72
Label IoI	102681	296.22	102718	296.09	102767	295.92	102814	295.87	102858	295.93
Label III	101812	296.77	101892	296.45	101893	296.24	102017	296.51	102081	297.38
Label IIII	101888	296.4	101930	296.1	101976	295.7	102034	295.8	102082	296.6
Mean	102293	297.0	102334	296.0	102379	296.0	102440	296.0	102499	296.0
Standard deviation	395	0.4	381	0.5	391	0.5	371	0.4	372	0.6
Span	869	1.1	826	1.4	874	1.5	797	1.2	778	1.8

Pressure mean value was quite stable, and the mean of the means was 102389Pa, with a small value of deviation, no bigger than 0.4%. The maximum pressure span was found to be 873Pa, much lower than the sensor individual uncertainty, which allows to define that this sensor uncertainty could be improved. Based on the presented values, it can be assumed that the outlet pressure was approximately constant, as the turbine diskharge was against the environment (101325Pa).

Temperature mean Standard deviation was about ±0.5K, which is close to the sensor individual uncertainty. In the other hand, temperature span was about 1.4K.

4.3 AIR MASS FLOW RATE, AND CHOCKED FLOW CONDITIONS

Mass flow rates were calculated by combining results from volumetric flow rates measured by a venturi sensor and air density, as a function of local and temperature values, from Table 4. Table 5 summarizes results calculated following NBR 5167-1:2008.

Table 5. Air mass flow rates and respective combined uncertainties calculated for 5 inlet absolute pressure levels and fixed temperature

Run	**1 (200 kPa)**	**2 (250 kPa)**	**3 (300 kPa)**	**4 (350 kPa)**	**5 (400 kPa)**
Unit	**kg/s**	**kg/s**	**kg/s**	**kg/s**	**kg/s**
Label 0	0.01474 ± 0.00262	0.01803 ± 0.0022	0.02153 ± 0.00194	0.02501 ± 0.00179	0.02867 ± 0.00172
Label I	0.01506 ± 0.00258	0.01858 ± 0.00216	0.02225 ± 0.00191	0.02566 ± 0.00178	0.02902 ± 0.00173
Label II	0.01471 ± 0.00261	0.01836 ± 0.00216	0.02213 ± 0.0019	0.02568 ± 0.00177	0.02919 ± 0.00172
Label I0I	0.01467 ± 0.00264	0.01851 ± 0.00217	0.02197 ± 0.00193	0.02573 ± 0.00178	0.0291 ± 0.00173
Label IoI	0.01455 ± 0.00266	0.01817 ± 0.0022	0.02187 ± 0.00193	0.02533 ± 0.00179	0.02888 ± 0.00173
Label III	0.01474 ± 0.00261	0.01849 ± 0.00216	0.02228 ± 0.0019	0.02581 ± 0.00177	0.02916 ± 0.00172
Label IIII	0.01474 ± 0.00261	0.01849 ± 0.00216	0.02227 ± 0.0019	0.0258 ± 0.00177	0.02916 ± 0.00172
Mean	0.014744	0.0183757	0.022043	0.025574	0.029026
Standard deviation	0.000155	0.000203	0.000276	0.000296	0.000190
Span	0.000510	0.000550	0.000750	0.000800	0.000520

It can be noted that the mass flow rate can be considered stable or constant in respect to each pressure level,. In respect to each of the rotor assembling, mass flow rate presented an increasing trend as a function of pressure level. Standard deviation and span can be considered as at the same order of magnitude, and less important than the individual combined measurement uncertainty, which has its values dictated by *PD-01* and *PT-02* uncertainties. The individual combined measurement uncertainty is displayed in Fig. 6.

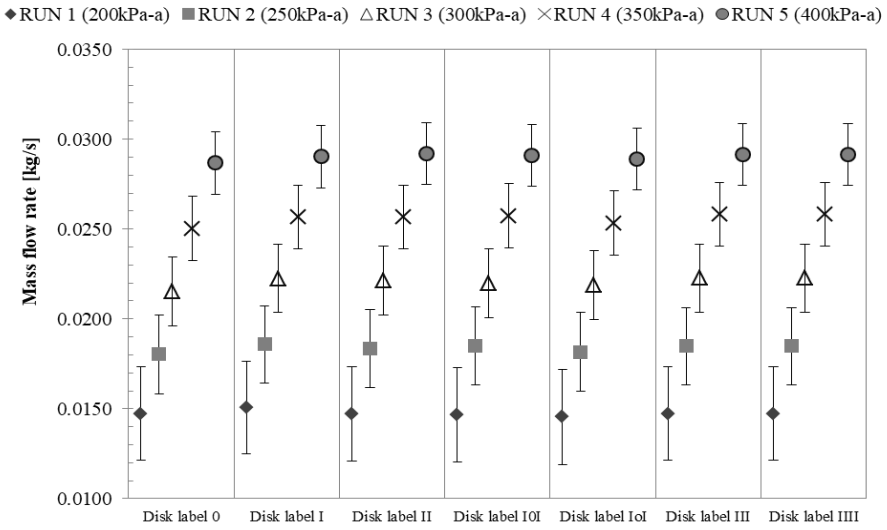

Figure 6. Measured mass flow rate with uncertainties

Combined uncertainty become smaller as the mass flow rate increase, due to the fixed full scale value of ± 50Pa associated to the measurement of the differential pressure in the Venturi tube. It is worth noticing that uncertainty ranges can show overlapping along the same pressure level, but they represent 5.9% to 17.8% of the mean measured mass flow rate value, which is acceptable for Venturi devices. Air flow can be considered at choked flow condition, because flow rate values were as constant for each of the pressure levels.

4.4. TYPE- A PERFORMANCE

The static torque for Type A set of tests, with variable number of disks, is presented in Table 6.

Table 6. Type A static torque values and combined uncertainties

Run	1 (200kPa)	2 (250kPa)	3 (300kPa)	4 (350kPa)	5 (400kPa)
Unit	Nm	Nm	Nm	Nm	Nm
Label 0	0.2943±0.0024	0.4169±0.0033	0.5396±0.0043	0.6622±0.0053	0.7971±0.0064
Label I	0.4047±0.0033	0.5886±0.0047	0.7725±0.0062	0.9442±0.0076	1.128±0.0091
Label II	0.4169±0.0034	0.6009±0.0048	0.7848±0.0063	0.9687±0.0078	1.14±0.0092
Label III	0.3556±0.0029	0.5641±0.0046	0.7848±0.0063	0.9933±0.008	1.226±0.0099
Label IIII	0.466±0.0038	0.6622±0.0053	0.8584±0.0069	1.03±0.0083	1.202±0.0097
Torque difference (Label IIII- Label 0)	0.2943±0.0024	0.4169±0.0033	0.5396±0.0043	0.6622±0.0053	0.7971±0.0064

Torque values were calculated from Eq. (1), with their combined uncertainties. Torque values can be considered as directly dependent to the number of disks (from label 0 to label IIII). Values for Label III at run 1, 2 and 5 (200kPa, 250kPa and 400 kPa) showed smaller values than some of the results for previous values (with less disks). Table botton line presents the static torque difference between Label IIII and Label 0, with 4 disks and no internal disk, respectively, indicating a 50% increase in torque values for that range. Combined uncertainties for static torque were all quite small, below 1%.

4.4. TYPE- B PERFORMANCE

Type B test was performed for 2 disk rotors, assembled in 3 spacing combination. Static torque values and combined uncertainties are presented in Table 7

Table 7. Type B static torque values and combined uncertainties

Run	1 (200kPa)	2 (250kPa)	3 (300kPa)	4 (350kPa)	5 (400kPa)
Unit	Nm	Nm	Nm	Nm	Nm
Label IoI	0.3556±0.0029	0.5396±0.0044	0.7112±0.0057	0.8829±0.0071	1.055±0.0085
Label II	0.4169±0.0034	0.6009±0.0048	0.7848±0.0063	0.9687±0.0078	1.1400±0.0092
Label I0I	0.3679±0.003	0.5641±0.0046	0.748±0.006	0.9687±0.0078	1.1650±0.0094
Torque span	0.0613	0.0613	0.0736	0.0858	0.1100

Label II stands for regularly distributed disks inside the rotor, and displayed some of the highest values of static torque, when compared to the 2 other distributions. Label IoI presented the poorest performance. Nevertheless, one individual result for Label II at run 5 displayed a static torque slightly smaller than the one expected. Combined uncertainties were all quite small, less than 1% of the nominal static torque values.

4.5 STATIC TORQUE BEHAVIOR AS FUNCTION OF THE INLET PRESSURE

Fig. 7 presents the static torque behavior as function of the inlet air pressure for the proposed rotor configuration, and presents three trend lines: Line 1refers to Label 0, Line 2 colects all data all excluding Label 0 and Line 3 takes into account all data with no exclusion.

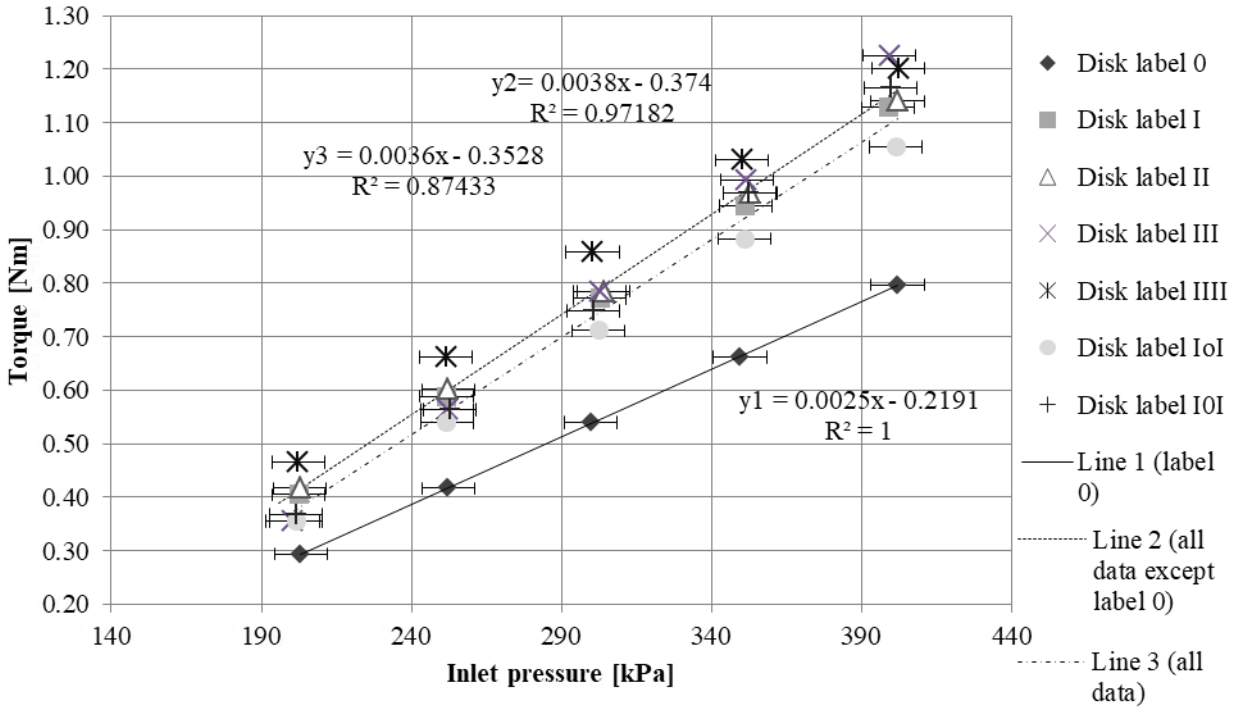

Figure 7. Static torque vs. inlet air pressure for 7 disk assemblings.

Regression lines show that the static torque displayed a linear relation in respect to the inlet air pressure, with their respective R^2 coefficients pretty close to 1 (1.00, 0.87 and 0.97 for lines 1, 2 and 3). The combined static torque uncertainty were found to be lower than 1%, which justifies its uncertainty bar to be neglected. Rotor assembled without any disk (Label 0/Line 1) showed the lowest torque conversion, and Disk IIII the highest one. All other disk configurations achieved intermediate torque convestion.

5. CONCLUSIONS

The main objective of this work was to identify static torque behavior for several rotor configurations, with different number of disks and relative spacing.. A Multiple Disk Turbine prototype was tested under laboratory conditions, driven by compressed air as the working fluid. Inlet air ranged from 200kPa to 400kPa and controlled temperature. Static torque was measured at rotor zero angular speed in order to identify turbine basic behaviors.

Assessment of the workbench performance to control the inlet thermodynamic properties was performed and results showed that inlet pressure control capacity presented a good behavior, since the pressure span was lower than the sensor uncertainty. For the inlet temperature an opposite behavior was observed, once the temperature span was higher then instrument uncertainty.

It was noticed that the effect of pressure increase has the higher influence in torque behavior, leading to 150% - 245% augmentation. Experiment showed a linear dependency of static torque with pressure, as expected for turbines with a choked flow condition.

The increment on the number of disks, assessed in Type A essays, showed an increment of 50% in torque values within the same air inlet pressure level, or run. Whenever the disk position were tested (Type B essays), it was observed a smaller variation in the static torque, from 10% to 17% Although of smaller influence, disk position can play an important role towards performance enhancement. Finally, it was found that through varying the inlet pressure and disk configuration, static torque increased from 0.28Nm to 1.2Nm, which is a rise of 4 times its initial value.

Analytical or numerical approaches could help to better understand the turbine behavior, and the experimental data reported in thos work will be of great value to develop such an assessment.

6. ACKNOWLEDGMENTS

Thomazoni acknowledges CNPq for his Dr grant; Antequera acknowledges CAPES for his MSc grant; Smith Schneider acknowledges CNPq for his research grant (PQ 305357/2013-1).

7. REFERENCES

ABNT NBR, ISO 5167-1:2008, 2008. “Medição de vazão de fluídos por dispositivos de pressão diferencial, inserido em condutos forçados de seção transversal circular”, <http://www.abntcatalogo.com.br/norma.aspx?ID=001541>.

Cairns, W. M. J., 2003. “The Tesla Disk”, 1 vols. Barrow Farm, Rode, Frome, Somerset: Camden Miniature Steam Services, Great Britain, 2nd edition

Carvalho, F., Machado da Rosa, L. and Schneider, P. S., 2017. “CFD Flow Analysis of a Tesla Turbine Under Motionless Regime”, 24th ABCM International Congress of Mechanical Engineering, COBEM, Brazil.

Ermel, C., Thomazoni, A., Rech Ch., Vieira, J., Novo, G. and Schneider, P. S., 2017. “Experimental Setup For a Bench Scale Multiple Disk Turbine (Tesla Turbine)”, 24th ABCM International Congress of Mechanical Engineering, COBEM, Brazil.

Couto, H. S., Duarte, J. B. F. and Bastos-Netto, D., 2006. “The Tesla Turbine Revisited”, 8° Asia-Pacific International Symposium on Combustion and Energy Utilization, Sochi.

Emram, T. A., 2011. “Tesla turbine torque modeling for construction of a dynamometer”, Master’s degree thesis, University of North Texas, USA.

Hasan, A. M., 2016. “Investigating the possibility of using a Tesla turbine as a drive unit for an automotive air-conditioning compressor using CFD modeling” The Free Library.

Holland, K., 2015 “Design, construction and testing of a Tesla Turbine”, Ph.D. thesis, Laurentian Université, Canada.

Lemma, E., Deam, R. T., Toncich, D., and Collins, R., 2008. “Characterization of a small viscous flow turbine”, Experimental Thermal and Fluid Science, vol. 33, n°33, p. 96–105, 2008.

Maidana, C. F., 2015. “Desenvolvimento de Turbinas de Múltiplos Diskos Estudo de Modelos Analíticos e Análise Experimental”, Ph.D. thesis, Universidade Federal do Rio Grande do Sul, Porto Alegre, Brazil.

Rice, R., 1965 “An Analytical and Experimental Investigation of Multiple-Disk Turbines”, Journal of Engineering for Power, v.87.

Sengupta, S.; Guha A., 2012. “A theory of Tesla disk turbines”, Proceedings of the Institution of Mechanical Engineers, Part A: Journal of Power and Energy, v. 226, n. 5, p. 650-663

Tesla, N., “Turbine” 1 061 206, 06-May-1913.

Truman, C. R., Jankowski, D.F., 1985. “Prediction of turbulent source flow between stationary and rotating disks”. Int. J. Heat & Fluid Flow.

Usman Saeed Khan M., Irfan Maqsood M., Ali E., Jamal S. and Javed M., 2013. “Proposed applications with implementation techniques of the upcoming renewable energy resource, The Tesla Turbine”. Journal of Physics: Conference Series, v. 439, n. 1, p. 012040.

8. RESPONSIBILITY NOTICE

The authors are the only responsible for the printed material included in this paper.

9. APPENDIX A

Table A.1. Measured data for all runs during the tests

Label 0												
RUN	**PT-01**		**TT-01**		**LC-01**		**PT-02**		**TT-02**		**PD-01**	
	[Pa-a]	**±**	**[K]**	**±**	**[kg]**	**±**	**[Pa-a]**	**±**	**[K]**	**±**	**[Pa]**	**±**
1	203088.5	8823	296.81	0.48	0.24	0.0001	102467.4	12571.58	296.66	0.61	144.04	50.9
2	252221.8		297.13		0.34		102459.5		296.78		215.94	
3	299759.2		296.72		0.44		102512.6		296.37		307.57	
4	349545.2		296.64		0.54		102555		296.69		415.86	
5	402056.1		296.9		0.65		102628.5		297.55		548.79	
Label I												
RUN	**PT-01**		**TT-01**		**LC-01**		**PT-02**		**TT-02**		**PD-01**	
	[Pa-a]	**±**	**[K]**	**±**	**[kg]**	**±**	**[Pa-a]**	**±**	**[K]**	**±**	**[Pa]**	**±**
1	202489.7	8823	297	0.48	0.33	0.0001	102628.8	12571.58	296.65	0.61	150.18	50.9
2	251692.5		296.74		0.48		102669.5		296.39		228.38	
3	302794.6		296.56		0.63		102715.2		296.21		327.79	
4	351323.3		296.39		0.77		102756.9		296.04		436.18	
5	398852.6		296.38		0.92		102813.4		296.03		558.44	
Label II												
RUN	**PT-01**		**TT-01**		**LC-01**		**PT-02**		**TT-02**		**PD-01**	
	[Pa-a]	**±**	**[K]**	**±**	**[kg]**	**±**	**[Pa-a]**	**±**	**[K]**	**±**	**[Pa]**	**±**
1	202797.6	8823	297.52	0.48	0.29	0.0001	101937.7	12571.58	297.17	0.61	144.47	50.9
2	252311.3		297.3		0.44		101987.8		296.95		225.11	
3	304053		297.04		0.58		102051.8		296.69		326.84	
4	352975.7		296.86		0.72		102113.6		296.51		440.24	
5	401980.9		296.76		0.86		102172.4		296.41		569.71	
Label I0I												
RUN	**PT-01**		**TT-01**		**LC-01**		**PT-02**		**TT-02**		**PD-01**	
	[Pa-a]	**±**	**[K]**	**±**	**[kg]**	**±**	**[Pa-a]**	**±**	**[K]**	**±**	**[Pa]**	**±**
1	201516	8823	296.42	0.48	0.3	0.0001	102638.5	12571.58	296.07	0.61	142.17	50.9
2	252849.6		295.91		0.46		102679.3		295.56		226.2	
3	300645.8		295.59		0.61		102738.2		295.14		318.39	
4	352584.4		295.73		0.79		102791.3		295.48		437.7	
5	399788.2		295.97		0.95		102859.3		295.72		560.7	
Label IoI												
RUN	**PT-01**		**TT-01**		**LC-01**		**PT-02**		**TT-02**		**PD-01**	
	[Pa-a]	**±**	**[K]**	**±**	**[kg]**	**±**	**[Pa-a]**	**±**	**[K]**	**±**	**[Pa]**	**±**
1	201605	8823	296.57	0.48	0.34	0.0001	102681.1	12571.58	296.22	0.61	139.91	50.9
2	251834.3		296.44		0.49		102718.2		296.09		218.22	
3	302329.1		296.27		0.64		102766.7		295.92		316.21	
4	351142.5		296.22		0.79		102814.3		295.87		424.34	
5	401480		296.28		0.93		102857.6		295.93		552.85	

Table A.1. Measured data for all runs during the tests (cont.)

Label III												
RUN	**PT-01**		**TT-01**		**LC-01**		**PT-02**		**TT-02**		**PD-01**	
	[Pa-a]	**±**	**[K]**	**±**	**[kg]**	**±**	**[Pa-a]**	**±**	**[K]**	**±**	**[Pa]**	**±**
1	202309.6	8823	297.12	0.48	0.29	0.0001	101811.6	12571.58	296.7	0.61	156.53	50.9
2	251520.6		296.8		0.46		101892.1		296.4		236.32	
3	300359.6		296.59		0.64		101893.2		296.2		331.06	
4	350161.4		296.86		0.81		102017.1		296.5		444.1	
5	402270.6		297.33		1		102081.1		297.3		578.71	
Label IIII												
RUN	**PT-01**		**TT-01**		**LC-01**		**PT-02**		**TT-02**		**PD-01**	
	[Pa-a]	**±**	**[K]**	**±**	**[kg]**	**±**	**[Pa-a]**	**±**	**[K]**	**±**	**[Pa]**	**±**
1	200377.3	8823	296.76	0.48	0.38	0.0001	101887.6	12571.58	296.4	0.61	144.76	50.9
2	251999.5		296.43		0.54		101929.6		296.1		227.72	
3	302861.5		296.03		0.7		101975.7		295.7		330.56	
4	351719.7		296.15		0.84		102033.6		295.8		444.02	
5	399400.1		296.98		0.98		102082.1		296.6		569.28	